An effective selenium-based fluorescence chemosensor for selective recognition of Hg^{2+} in aqueous medium: experimental and theoretical studies

Puthiyavalappil Rasin -
National Institute of Technology Tiruchirappalli
Moideen Musthafa -
National Institute of Technology Tiruchirappalli
Anandaram Sreekanth - (sreekanth@nitt.edu)
National Institute of Technology Tiruchirappalli

Research Article

Keywords: Fluorescence chemosensor, Mercury, Selenourea, MEP, DFT

Posted Date: June 22nd, 2022

DOI: https://doi.org/10.21203/rs.3.rs-1745296/v1

Abstract

We introduce a novel selenium-based compound [N-(Phenylcarbamoselenoyl) furan-2-carboxamide] for the optical and fluorimetric detection of Hg in an aqueous medium. The synthesized compound was characterized by different spectroscopic methods. The designed chemosensor FSU has shown a significant fluorescence quenching when Hg^{2+} ions were added to the sensing medium. Furthermore, Hg^{2+} ions provoked a 2:1 complex formation with the chemosensor FSU. It is found that the compound offers high selectivity over a variety of cations such as Co^{2+}, Cr^{3+}, Ni^{2+}, Zn^{2+}, Cu^{2+}, Mg^{2+}, Hg^{2+}, Cd^{2+}, Ca^{2+}, Mn^{2+}, Ga^{3+}, Pb^{2+}, Na^{+}, Fe^{2+} and K^{+}. The detection limit was calculated as 7.35×10^{-7} M. Also, FSU shows appreciable binding affinity towards Hg^{2+} ions with a binding constant value of 1.413×10^{3} M^{-1}. The ICT mechanism of mercury sensing was confirmed with spectroscopic techniques and DFT studies. Density functional theory was also implemented to investigate the structure of the Hg^{2+} complex and its electronic distribution in the aqueous medium. Finally, an MEP study was also carried out to obtain detailed information about the surface characteristics of the chemosensor FSU. Effectively, we have reported a potent chemosensor for Hg^{2+} in the aqueous medium.

Introduction

Mercury (Hg) is a toxic heavy metal found in the earth's crust including deposits of coal. Over the past century, levels of mercury in the atmosphere keep increasing to a significant extent due to volcanic eruptions and the liberation of mercury from hydroelectric mining and paper industries [1–3]. Furthermore, unscientific and inappropriate disposal of municipal and medicinal wastes causes mercury emissions in the environment [4–5]. Similarly, thermal power plants using coal as a fuel also contribute to excess mercury emission [6]. Various forms of mercury can exist mainly in elemental, inorganic and organic forms (methyl mercury). Mercury in its elemental form is mainly released through sewage discharge and sediment, furthermore from agricultural processes, household, commercial and medical products containing mercury [7]. Oxidation of elemental mercury leads to the formation of inorganic mercury, which is used in the field of batteries [8–9]. Organic mercury, often called methyl mercury, is produced by some bacterial organisms in the water that convert inorganic mercury into organic mercury [10].

Among the hazardous chemicals, organic mercury compounds are well-known and highly toxic. Long-term exposure to methyl mercury causes serious health problems. Accumulation of mercury in organisms creates harmful effects at the top of the food chain. Consumption of species belonging to the upper level of the food chain can cause mercury deposition in the brain and kidney, which finally results in neurological and nephrological disorders [11–15]. Being a soft metal, mercury can easily bind with the sulfur present in many enzymes and proteins, and hence cause direct damage to cells and their functions [16–18]. Therefore, detecting and controlling the amount of mercury in the environment is an important task that has to be done for the well-being of humans and other organisms.

Several methods are available for the quantitative and qualitative determination of mercury including the use of sophisticated instruments such as atomic emission spectroscopy, atomic absorption spectroscopy, and inductively coupled plasma [19]. Even though these instruments have high sensitivities towards mercury in the environment, the actual forms of mercury are destroyed while using these techniques [20]. In other words, detection of mercury using instruments may include all forms of mercury such as Hg^0, Hg^{2+}, CH_3Hg, and other organic mercury compounds. So, it is difficult to differentiate different forms of mercury in various samples using instrumental related methods. Unlike these techniques, many chemical sensors have proven to be effective for analyzing various forms of mercury in different samples. Usually, these sensors are used to detect abiotic mercury. Since a huge amount of mercury in the environment is abiotic, chemical sensors are the perfect tools to monitor mercury levels in the environment [21]. High sensitivity, long lifetime, and low costs make this technique more accessible and convenient in mercury detection.

Based on the factors mentioned above, we have designed and developed a new selenoureas derivative for the detection of mercury in water. As per the available report to date, selenium acts as a magnet towards mercury [22]. Also being a soft metal, selenium has a greater tendency to interact with mercury [23]. The synthesized compound was confirmed by using different spectroscopic methods. To have a better understanding of the structural properties of the prepared compound, computational studies were conducted using DFT calculations, from which we calculated the HOMO-LUMO energy gap and interconnected parameters. In this paper, we give a detailed account of the individual steps leading to the formation of selenourea and its derivative for the optical and fluorescent sensing of mercury (II).

Materials And Methods

Chemicals and instruments

Analytical reagent (AR) grade chemicals were purchased for this study from the suppliers and used as received. Different metal chlorides (Co^{2+}, Cr^{3+}, Ni^{2+}, Zn^{2+}, Mg^{2+}, Cu^{2+}, Hg^{2+}, Cd^{2+}, Ca^{2+}, Mn^{2+}, Ga^{2+}, Pb^{2+}, Na^{+}, Fe^{2+} and K^{+}) were taken to investigate the sensing property of the compound (FSU). All the studies were conducted using double distilled water. Various spectroscopic techniques were used to characterize the chemosensor (FSU) and the complex (FSU-Hg^{2+}). The proton and ^{13}C NMR spectra were produced on a Bruker, 500 MHz in DMSO-d6 at 298 K with TMS as an internal standard. FT-IR spectra of both chemosensor FSU and FSU-Hg^{2+} complex were obtained using a Perkin-Elmer FT-IR spectrophotometer in the range of 400-4000 cm^{-1}. UV-Vis diode-array spectrometer (Analytical Jena specords 600) was used to generate UV-Visible spectra of compounds. Also, emission spectra were produced and analyzed using a spectrofluorometer (Jasco V-630). Mass spectra analysis of the chemosensor (FSU) and complex (FSU-Hg^{2+}) was done with the help of an Agilent mass spectrometer.

Preparation of the chemosensor (FSU)

The aniline substituted selenourea ([N-(Phenylcarbamoselenoyl) furan-2-carboxamide]) (FSU) was prepared and purified by referring to previous year's publications [24-25]. The compound was synthesized with a good yield. The procedure for the synthesis of chemosensor FSU is provided in the supplementary file.

Fluorescent studies of the receptor (FSU)

5 mL of $8x10^{-3}$ M solution of the chemosensor (FSU) was made in DMSO/water system by dissolving 11.72 mg and further decreasing the concentration to $8x10^{-5}$ M. The fluorescent properties of the chemosensor (FSU) ($8x10^{-5}$) were investigated in DMSO/water (95/5 v/v) and the emission was observed at the wavelength of 440 nm. Different metal chlorides have been used for this sensing study. Aqueous solutions of different metal salts are made in Millipore water at a concentration of $8x10^{-3}$ M. The excitation wavelength of the chemosensor (FSU) was observed to be 305 nm.

To have a better insight into the sensing properties of the chemosensor (FSU) towards Hg^{2+}, fluorescent titration experiments were implemented at 440nm. The detection limit (LOD) value of the chemosensor (FSU) was calculated using the equation 3σ/K (where σ represents standard deviation and the slope of the calibration plot is denoted by K). The selectivity, as well as the interference studies, were performed for the chemosensor (FSU) towards Hg^{2+} by exciting at 305 nm with the co-existing metal cations.

DFT calculations

Theoretical DFT studies have been performed for compounds (FSU and FSU-Hg^{2+}) to investigate the electronic behavior of the individual atoms using the B3LYP/ 6-31G (d, p)/LanL2DZ level of theories. Also, using molecular electrostatic potential map (MEP) studies, the electron density of the surface was predicted. Furthermore, this study was also used to find the parameters like chemical reactivity and the energy corresponding HOMO and LUMO orbitals of the chemosensor (FSU) and FSU-Hg^{2+} complex.

Results And Discussion

Preparation of the chemosensor (FSU)

The chemosensor [N-(Phenylcarbamoselenoyl) furan-2-carboxamide] was synthesized and characterized by referring to a procedure reported previously and then purified by column chromatography. The compound (FSU) is a brown-colored solid, stable in air, non-hygroscopic, and shows better solubility in dimethyl sulphoxide (DMSO). The general protocol for the synthesis of FSU is summarized in **scheme 1**.

The derivative of selenourea (FSU) was synthesized with a good yield. Elemental analysis and other spectroscopic tools were used to characterize the compound. Electronic spectra of the FSU described an absorption peak around 305 nm ($\pi \rightarrow \pi^*$).The bands that appeared approximately at a range of 3263 cm^{-1} for amide N–H were highlighted in the FT-IR spectra of FSU. The Selenourea N–H was observed at

3118 cm^{-1} and this value is shifted to a lower region of wavenumber, it can be explained based on the hydrogen bonding between N–H of Selenourea and the carbonyl oxygen. The C=O frequency for FSU was observed at 1665 cm^{-1} region. The characteristic absorption band of C=Se vibrations appeared at the range of 1274 cm^{-1} which agreed with the previously reported selenourea compounds [26]. In the ^{1}H NMR spectra of FSU, the N–H proton which is present in between carbonyl and selenocarbonyl groups appeared as singlets around 10.89 ppm and the peak appeared at the range of 10.56 ppm was assigned to N–H proton which is attached between selenocarbonyl and phenyl ring. All other peaks corresponding to the aromatic protons were observed at the expected region (6.75-8.50 ppm). The entire characterization data mentioned above is represented in **Fig.S1 to S4**.

Fluorescence studies

The efficiency of a chemosensor is usually discussed based on its selectivity. The present work reveals the ability of the chemosensor FSU to detect Hg^{2+} ion in presence of different metal cations such as Co^{2+}, Cr^{3+}, Ni^{2+}, Zn^{2+} Mg^{2+}, Cu^{2+}, Mn^{2+}, Ca^{2+}, Cd^{2+}, Ga^{3+}, Pb^{2+}, Fe^{2+}, Na^{+}, and K^{+} of 10-fold excess in concentration in the reaction medium. As described in **Fig. 1a**, only Hg^{2+} ion can induce a significant fluorescence quenching at 440 nm in the presence of various cations in the FSU solution. Other cations are not capable enough to produce a significant variation in the fluorescence intensity of chemosensor FSU. Apart from this, metal ions' interference studies were also performed. As described in **Fig. 2a**, even after the addition of different cations to the complex FSU-Hg^{2+} system, the emission intensity almost remains constant. This clearly indicates that the recognition process of Hg^{2+} is not influenced by other cations. As mentioned previously, the chemosensor FSU was specific to the detection of Hg^{2+} ions. Furthermore, the time of response study for the chemosensor FSU towards Hg^{2+} was studied (**Fig. S6**). The emission intensity of the complex FSU-Hg^{2+} remains almost the same at different time intervals (0-180s), indicating that the complex formed is stable.

The effect of pH in the sensing of Hg^{2+} ions was also investigated by conducting pH study within the range of 1 to 14 (**Fig. S5**). Hydrochloric acid and sodium hydroxide solutions were used to adjust the pH of the sensing medium. The fluorescent intensity of the chemosensor FSU was almost constant in the preferred pH range describing its consistency. The fluorescence emission intensity of the FSU-Hg^{2+} complex gradually increases and reaches maximum at a pH of 4. When the pH was shifted from acidic to neutral in the range of 6 to 9, fluorescence intensity decreased and that may due to the maximum interactions occurred between selenium and mercury in neutral medium. Also, in basic medium the fluorescence intensity of the system increased slightly that reveals the less stability FSU-Hg^{2+} complex in basic pH. So the results of pH study reveals that the FSU-Hg^{2+} system is stable in neutral pH rather than acid and basic pH. So all the fluorescence studies were conducted in aqueous pH.

Fluorescence titration experiments were performed (**Fig. 2b**) to get a better insight into the mechanism of sensing and detection limit. **Fig. 2b** demonstrated that the fluorescence emission of the chemosensor FSU at 440 nm was decreasing upon the successive addition of ($8x10^{-5}$ M) Hg^{2+} solution in water (0-1.6

equivalents). The fluorescence intensity of the chemosensor FSU remains unchanged even after 1.6 equivalents of Hg^{2+} ions were added and after that quenching was not observed even the amount of the Hg^{2+} ion raised in the medium. The chemosensor fsu can be recommended as a good candidate for mercury (II) ion sensing due to its ability to quench the fluorescence intensity of FSU.

A calibration plot was constructed between Hg^{2+} ion concentration and the fluorescence emission values (y=0.9830) (**Fig. 3**). The equation 3σ/K was used to determine the detection limit of the chemosensor FSU towards Hg^{2+} ion and it was found to be 7.35×10^{-7} M which is lower than the detection limits of many reported sensors for Hg^{2+} ion (Table S1) [S.I 27-32]. When this value is compared with the value reported by WHO, it is below the acceptable limit of Hg^{2+} in drinking water [33]. Also, the correlation constant value was found to be 1.413×10^{3} M^{-1} using the B-H equation developed from the titration values (**Fig. 4**). Thus, the results mentioned above described that the chemosensor FSU is a better chemical tool for the sensing of Hg^{2+} ions and a standard plot was developed with better linearity (R2=0.9871) for the quantitative analysis of mercury.

Further confirmation of the chemosensor metal complex was done by means of a mass analyzer. The HR-MS spectra confirmed the formation of ligand (FSU) and the complex FSU-Hg^{2+}. The peak observed at M/Z = 922.009 corresponds to [M+ACN+Na^{+}] where M= FSU-Hg^{2+} **(Fig. 5)** and which further reveals the 2:1 ratio of chemosensor and metal ions. Fluorescent titration values were used to build the Job's diagram (**Fig. 6**) and it was further used to confirm the 2:1 ratio of chemosensor and Hg^{2+} ions. As mentioned in **Fig. 6**, two straight lines meet at a point where the mole fraction is 0.4, which confirms the 2:1 (ligand to mercury) stoichiometry of complex formation between the chemosensor (FSU) and Hg^{2+} [34].

The plausible binding mechanism of the FSU-Hg^{2+} complex (**Fig.8**) was proposed based on, the FT-IR, NMR titration and DFT calculation studies. The fluorescence property of the chemosensor FSU can be explained based on the ICT process taking place within the compound [35-36]. While upon the addition of Hg^{2+} to the chemosensor, the ICT process was interrupted and that resulted in fluorescence quenching. Since, there was no significant change in the chemical shift values of the –NH protons, the ^{1}H NMR titration study clearly suggested that the –NH moieties were not involved in coordination with the mercury ions (**Fig. 7**). It was further confirmed by the FT-IR analysis. The FT-IR spectra of both FSU and the complex FSU-Hg^{2+} were recorded (**Fig. S3)**. From the spectra, it is clear that except for –C=Se moiety, the stretching frequencies of all other functional groups remain almost the same. After the addition of Hg^{2+} - C=Se stretching frequency was lowered from 1274 cm^{-1} to 1250 cm^{-1} thereby confirming the direct interaction of selenium and mercury.

We also carried out the reversibility study of the chemosensor FSU, because it is also important when one considers its metal ion sensing application. The FSU-Hg^{2+} complex (8×10^{-5} M^{-1} - 1×10^{-3} M) in DMSO/ water (95/5, v/v) system was reversed by EDTA addition (2.0×10^{-3} M). The Hg^{2+} complex formation

with the chemosensor FSU disappeared after the addition of EDTA (**Fig. S7**), showing the reversible sensing action.

DFT calculations

In order to verify the results obtained experimentally, density functional theory was executed for both chemosensor FSU and FSU-Hg^{2+} complex using the Gaussian 09 software with B3LYP/ 6-31G (d, p)/LanL2DZ level of theory. The optimized structures of the chemosensor FSU and the complex FSU-Hg^{2+} are depicted in **Fig. 9**. The density functional theory calculations clearly described that the electron density of FSU is mainly distributed in the region of –C=Se and –C=O at HOMO and LUMO energy levels. After the complexation of FSU with Hg^{2+}, the electron density around –C=O and –C=Se decreased significantly and shifted towards Hg^{2+}. These results demonstrated that electron transfer occurred within the chemosensor and it was blocked by the addition of Hg^{2+} which resulted in weak fluorescence intensity. As depicted in the Figure (**Fig. 9**), the HOMO-LUMO for chemosensor FSU and the complex FSU-Hg^{2+} were found to be 0.1134 and 0.1001 eV respectively. Critical chemical reactivity parameters like softness, hardness (η), electronegativity (χ), chemical potential (μ), electron-affinity (A), and ionization energy (I) were calculated based on the HOMO-LUMO energy gap. These properties have been defined as follows [37].

$$\eta = (I-A)/2 \qquad \mu = -(I-A)/2 \qquad \chi = (I+A)/2$$

Where I and A were obtained from HOMO and LUMO energies as $I = -E_{HOMO}$ and $A = -E_{LUMO}$ as per Janak theorem and Perdew et al. [38].

Table 1. Calculated energy values for FSU using B3LYP/6-31G (d, p) basis set	
Parameters	
Energy (au)	-1537.22
Dipole moment (Debye)	6.1802
E_{HOMO} (eV)	-0.2095
E_{LUMO} (eV)	-0.1094
$E_{HOMO-LUMO}$ (eV)	0.1134
E_{HOMO-1} (eV)	-0.2177
E_{LUMO+1} (eV)	-0.1044
$E_{(HOMO-1)-(LUMO+1)}$ (eV)	0.1133
Hardness (η)	0.0567
Chemical Potential (μ)	-0.1595
Electronegativity (χ)	0.1595
Electrophilicity index (ω)	0.4487

Hardness (η) which is directly related to stability was found to be 1.7448 eV for FSU. The tendency of electrons to escape from an equilibrium system was termed chemical potential and that was found to be -3.7045 for FSU. The global electrophilicity index (ω), a global reactivity index that is related to η and μ, first introduced by Parr et al. [39]. It is the measure of the stabilization attained by the system in terms of energy when it acquired extra electronic charge from the surroundings and is given by $\omega = \mu^2/\eta$. The corresponding value for fsu is 7.8652 e.V. Receptor FSU provides a proper molecular structure to coordinate with the Hg^{2+} ion. The obtained results also revealed that the HOMO-LUMO energy gap corresponding to the complex FSU-Hg^{2+} was lower when compared to the chemosensor FSU thereby form a stable complex. A strong interaction between the chemosensor FSU and Hg^{2+} ions imparted a distortion of electronic structure of chemosensor FSU that led to the quenching of the fluorescent emission.

Molecular electrostatic potential (MEP) surface analysis

The MEP analysis is an effective theoretical tool for predicting reaction behaviour of molecules. MEP analysis allow us to envisage the distribution of electro cloud of compounds and provide other charge related properties. ESP study is one of the important theoretical methods by which organic chemists are analyzing the interactions among drug-receptor and enzyme-substrate along with hydrogen bonding interactions.

A comparative view of molecular electrostatic maps (MEP) is shown in **Fig. 10.** MEP of FSU was calculated using BL3YP/6-31G (d, p) basis set. The graphic representation with the rainbow colour scheme of ESP lies in the range of -6.018e-2 to +6.108e-2 for FSU. The high electron density (negative potential) indicates regions that are red colour. The low electron density (positive potential) indicates regions that are blue colour. As can be seen in the MEP for FSU, the three regions around carbonyl oxygen and carbonyl selenium of FSU are red and hence possess high electron density or in other words a site more exposed to electrophilic attack [40].

Conclusion

In this present study, we have successfully developed and characterized a new selenium-based fluorescent chemosensor for the detection of Hg(II) ion. Preparation of chemosensor FSU involves two-step process and exhibits a high affinity towards Hg(II) even in the presence of other metal ions in the sensing medium. A linear calibration curve of $1/(I_0\text{-}I)$ against $1/Hg^{2+}$ was developed with a correlation coefficient of 0.9871. The detection limit value was found as 7.35×10^{-7} M using the Eq. 3σ/K. HR-MS technique and Job's diagram were used to confirm the 2:1 molar ratio of the FSU-Hg^{2+} complex. Furthermore, DFT calculations were performed to verify the experimental results. The quenching constant value was calculated as 1.413×10^{3} M^{-1} thereby confirming the better sensing property of the chemosensor FSU towards Hg(II) ion.

Declarations

Acknowledgments

The author Puthiyavalappil Rasin is grateful to MHRD, Govt. of India for the financial support. The author would like to thank the National Institute of Technology Tiruchirappalli for the instrumentation facility.

Funding

The authors declare that during the preparation of this manuscript no funds or grants were received.

Conflicts of interest

No relevant financial or non-financial interests to disclose.

Ethics approval

Not applicable.

Consent to participate

Not applicable.

Consent to publish

Not applicable.

Availability of data and material

Not applicable (datasets were not generated or analyzed during the current study).

Code availability

Not applicable.

Authors' contributions

The present manuscript has been approved by all the authors listed in the manuscript. Synthesis and characterization of the chemosensor were done by Moideen Mustafa. The sensing and all other related studies were done by Puthiyavalappil Rasin. Also, the final draft of the manuscript was written by Puthiyavalappil Rasin. The guidance for this work and final corrections were done by Anandaram Sreekanth. Here we confirm that the authorships have been approved by all of us.

References

1. Hilson, G. Abatement of Mercury Pollution in the Small-Scale Gold Mining Industry: Restructuring the Policy and Research Agendas. *Sci. Total Environ.* **2006**, *362* (1–3), 1–14. https://doi.org/10.1016/j.scitotenv.2005.09.065.
2. Schuster, P. F.; Krabbenhoft, D. P.; Naftz, D. L.; Cecil, L. D.; Olson, M. L.; Dewild, J. F.; Susong, D. D.; Green, J. R.; Abbott, M. L. Atmospheric Mercury Deposition during the Last 270 Years: A Glacial Ice Core Record of Natural and Anthropogenic Sources. *Environ. Sci. Technol.* **2002**, *36* (11), 2303–2310. https://doi.org/10.1021/es0157503.
3. Rahman, Z.; Singh, V. P. The Relative Impact of Toxic Heavy Metals (THMs) (Arsenic (As), Cadmium (Cd), Chromium (Cr)(VI), Mercury (Hg), and Lead (Pb)) on the Total Environment: An Overview. *Environ. Monit. Assess.* **2019**, *191* (7). https://doi.org/10.1007/s10661-019-7528-7.
4. Manzoor, J.; Sharma, M. Impact of Biomedical Waste on Environment and Human Health. *Environ. Claims J.* **2019**, *31* (4), 311–334. https://doi.org/10.1080/10406026.2019.1619265.
5. Gupta Mamta. Environmental Effects of Growing E Waste. *Int. J. Sci. Res.* **2012**, *3* (12), 2319–7064.
6. Wang, S.; Zhang, L.; Wu, Y.; Ancora, M. P.; Zhao, Y.; Hao, J. Synergistic Mercury Removal by Conventional Pollutant Control Strategies for Coal-Fired Power Plants in China. *J. Air Waste Manag.*

Assoc. **2010**, *60* (6), 722–730. https://doi.org/10.3155/1047-3289.60.6.722.

7. Gochfeld, M. Cases of Mercury Exposure, Bioavailability, and Absorption. *Ecotoxicol. Environ. Saf.* **2003**, *56* (1), 174–179. https://doi.org/10.1016/S0147-6513(03)00060-5.
8. Park, J. D.; Zheng, W. Human Exposure and Health Effects of Inorganic and Elemental Mercury. *J. Prev. Med. Public Heal.* **2012**, *45* (6), 344–352. https://doi.org/10.3961/jpmph.2012.45.6.344.
9. von Burg, R. Inorganic Mercury. *Journal of Applied Toxicology*. 1995, pp 483–493. https://doi.org/10.1002/jat.2550150610.
10. Boening, D. W. *Ecological E€ects, Transport, and Fate of Mercury: A General Review*.
11. Hong, Y. S.; Kim, Y. M.; Lee, K. E. Methylmercury Exposure and Health Effects. *J. Prev. Med. Public Heal.* **2012**, *45* (6), 353–363. https://doi.org/10.3961/jpmph.2012.45.6.353.
12. Li, P.; Feng, X.; Qiu, G. Methylmercury Exposure and Health Effects from Rice and Fish Consumption: A Review. *Int. J. Environ. Res. Public Health* **2010**, *7* (6), 2666–2691. https://doi.org/10.3390/ijerph7062666.
13. Davis, J.; Yee, D.; Collins, J.; Schwarzbach, S.; Luoma, S. Potential for Increased Mercury Accumulation in the Estuary Food Web. *San Fr. Estuary Watershed Sci.* **2003**, *1* (1). https://doi.org/10.15447/sfews.2003v1iss1art4.
14. Baby, J.; Raj, J. S.; Biby, E. T.; Sankarganesh, P.; Jeevitha, M. V; Ajisha, S. U.; Rajan, S. S. \376\377\0007\0003\0000\000-\000l\000J\000B\000C\000S\000-\000A\000r\000t\000i\000c\000l\000e\000-\000 \000R\000a\000j\000 \000S\000t\000e\000p\000h\000y. **2010**.
15. Selid, P. D.; Xu, H.; Collins, E. M.; Face-Collins, M. S.; Zhao, J. X. Sensing Mercury for Biomedical and Environmental Monitoring. *Sensors* **2009**, *9* (7), 5446–5459. https://doi.org/10.3390/s90705446.
16. Ravichandran, M. Interactions between Mercury and Dissolved Organic Matter - A Review. *Chemosphere*. Elsevier Ltd 2004, pp 319–331. https://doi.org/10.1016/j.chemosphere.2003.11.011.
17. Patrick, L. *Patrick L. Mercury Toxicity and Antioxidants: Part 1: Role of Glutathione and Alpha-Lipoic Acid in the Treatment*.
18. Xu, F. F.; Imlay, J. A. Silver(I), Mercury(II), Cadmium(II), and Zinc(II) Target Exposed Enzymic Iron-Sulfur Clusters When They Toxify Escherichia Coli. *Appl. Environ. Microbiol.* **2012**, *78* (10), 3614–3621. https://doi.org/10.1128/AEM.07368-11.
19. Bersier, P. M.; Howell, J.; Bruntlett, C. Tutorial Review. Advanced Electroanalytical Techniques versus Atomic Absorption Spectrometry, Inductively Coupled Plasma Atomic Emission Spectrometry and Inductively Coupled Plasma Mass Spectrometry in Environmental Analysis. *Analyst* **1994**, *119* (2), 219–232. https://doi.org/10.1039/AN9941900219.
20. Leermakers, M.; Baeyens, W.; Quevauviller, P.; Horvat, M. Mercury in Environmental Samples: Speciation, Artifacts and Validation. *TrAC - Trends Anal. Chem.* **2005**, *24* (5), 383–393. https://doi.org/10.1016/j.trac.2004.01.001.

21. Namieśnik, J. Trends in Environmental Analytics and Monitoring. *Crit. Rev. Anal. Chem.* **2000**, *30* (2–3), 221–269. https://doi.org/10.1080/10408340091164243.
22. Ibrahim, A. T. A.; Banaee, M.; Sureda, A. Selenium Protection against Mercury Toxicity on the Male Reproductive System of Clarias Gariepinus. *Comp. Biochem. Physiol. Part - C Toxicol. Pharmacol.* **2019**, *225*. https://doi.org/10.1016/j.cbpc.2019.108583.
23. Lourdes, M. A.; Cuvin-Aralar, A.; Furness, R. W. *Mercury and Selenium Interaction: A Review*, 1991.
24. Musthafa, M.; Konakanchi, R.; Ganguly, R.; Balachandran, C.; Aoki, S.; Sreekanth, A. Synthesis, Characterization, Theoretical, Molecular Docking and in Vitro Biological Activity Studies of Ru(II) (H6 -p-Cymene) Complexes with Novel Aniline Substituted Aroyl Selenoureas. *J. Biomol. Struct. Dyn.* **2021**, *39* (12), 4346–4361. https://doi.org/10.1080/07391102.2020.1778531.
25. Hussain, R. A.; Badshash, A.; Sohail, M.; Lal, B.; Altaf, A. A. Synthesis, Chemical Characterization, DNA Interaction and Antioxidant Studies of Ortho, Meta and Para Fluoro Substituted Ferrocene Incorporated Selenoureas. *Inorganica Chim. Acta* **2013**, *402*, 133–139. https://doi.org/10.1016/j.ica.2013.04.003.
26. Musthafa, M.; Konakanchi, R.; Ganguly, R.; Pandikumar, P.; Sreekanth, A. Synthesis, Characterization, in Silico and in Vitro Biological Activity Studies of Ru(II) (η 6-p-Cymene) Complexes with Novel N-Dibenzosuberene Substituted Aroyl Selenourea Exhibiting Se Type Coordination. *Res. Chem. Intermed.* **2020**, *46* (8), 3853–3877. https://doi.org/10.1007/s11164-020-04177-w.
27. Hsieh, Y. C.; Chir, J. L.; Wu, H. H.; Chang, P. S.; Wu, A. T. A Sugar-Aza-Crown Ether-Based Fluorescent Sensor for Hg2 + and Cu2+. *Carbohydr. Res.* **2009**, *344* (16), 2236–2239. https://doi.org/10.1016/j.carres.2009.08.027.
28. Zhao, N.; Lam, J. W. Y.; Sung, H. H. Y.; Su, H. M.; Williams, I. D.; Wong, K. S.; Tang, B. Z. Effect of the Counterion on Light Emission: A Displacement Strategy to Change the Emission Behaviour from Aggregation-Caused Quenching to Aggregation-Induced Emission and to Construct Sensitive Fluorescent Sensors for Hg2 + Detection. *Chem. - A Eur. J.* **2014**, *20* (1), 133–138. https://doi.org/10.1002/chem.201303251.
29. Wu, X. F.; Ma, Q. J.; Wei, X. J.; Hou, Y. M.; Zhu, X. A Selective Fluorescent Sensor for Hg2 + Based on Covalently Immobilized Naphthalimide Derivative. *Sensors Actuators, B Chem.* **2013**, *183*, 565–573. https://doi.org/10.1016/j.snb.2013.04.024.
30. Weng, J.; Mei, Q.; Ling, Q.; Fan, Q.; Huang, W. A New Colorimetric and Fluorescent Ratiometric Sensor for Hg 2 + Based on 4-Pyren-1-Yl-Pyrimidine. *Tetrahedron* **2012**, *68* (14), 3129–3134. https://doi.org/10.1016/j.tet.2011.12.071.
31. Eroy-Reveles, A. A.; Mascharak, P. K. Screening Mercury Levels in Fish with a Selective Flourescent Chemosensor: Highly Selective Chromogenic and Redox or Fluorescent Sensors of Hg2 + in Aqueous Environment Based on 1,4-Disubstituted Azines. *Chemtracts* **2005**, *18* (8), 455–462.
32. Bozkurt, E.; Gul, H. I. A Novel Pyrazoline-Based Fluorometric “Turn-off” Sensing for Hg2+. *Sensors Actuators, B Chem.* **2018**, *255*, 814–825. https://doi.org/10.1016/j.snb.2017.08.062.

33. Pala, I. R.; Brock, S. L. ZnS Nanoparticle Gels for Remediation of Pb 2 + and Hg 2 + Polluted Water. *ACS Appl. Mater. Interfaces* **2012**, *4* (4), 2160–2167. https://doi.org/10.1021/am3001538.
34. Jing, S.; Zheng, C.; Pu, S.; Fan, C.; Liu, G. A Highly Selective Ratiometric Fluorescent Chemosensor for Hg2 + Based on a New Diarylethene with a Stilbene-Linked Terpyridine Unit. *Dye. Pigment.* **2014**, *107*, 38–44. https://doi.org/10.1016/j.dyepig.2014.03.023.
35. Tümay, S. O.; Uslu, A.; Ardiç Alidağı, H.; Kazan, H. H.; Bayraktar, C.; Yolaçan, T.; Durmuş, M.; Yeşilot, S. A Systematic Series of Fluorescence Chemosensors with Multiple Binding Sites for Hg(Ii) Based on Pyrenyl-Functionalized Cyclotriphosphazenes and Their Application in Live Cell Imaging. *New J. Chem.* **2018**, *42* (17), 14219–14228. https://doi.org/10.1039/c8nj02482k.
36. Sohrabi, M.; Amirnasr, M.; Meghdadi, S.; Lutz, M.; Bikhof Torbati, M.; Farrokhpour, H. A Highly Selective Fluorescence Turn-on Chemosensor for Zn2+, and Its Application in Live Cell Imaging, and as a Colorimetric Sensor for Co2+: Experimental and TD-DFT Calculations. *New J. Chem.* **2018**, *42* (15), 12595–12606. https://doi.org/10.1039/c8nj01580e.
37. Nataraj, A.; Balachandran, V.; Karthick, T. Molecular Orbital Studies (Hardness, Chemical Potential, Electrophilicity, and First Electron Excitation), Vibrational Investigation and Theoretical NBO Analysis of 2-Hydroxy-5-Bromobenzaldehyde by Density Functional Method. *J. Mol. Struct.* **2013**, *1031*, 221–233. https://doi.org/10.1016/j.molstruc.2012.09.047.
38. Stein, T.; Autschbach, J.; Govind, N.; Kronik, L.; Baer, R. Curvature and Frontier Orbital Energies in Density Functional Theory. *J. Phys. Chem. Lett.* **2012**, *3* (24), 3740–3744. https://doi.org/10.1021/jz3015937.
39. Domingo, L. R.; Pérez, P. Global and Local Reactivity Indices for Electrophilic/Nucleophilic Free Radicals. *Org. Biomol. Chem.* **2013**, *11* (26), 4350–4358. https://doi.org/10.1039/c3ob40337h.
40. Darroudi, M.; Mohammadi Ziarani, G.; Ghasemi, J. B.; Badiei, A. Facile and Green Preparation of Colorimetric and Fluorescent Sensors for Mercury, Silver, and Carbonate Ions Visual Detecting: Spectroscopy and Theoretical Studies. *J. Mol. Struct.* **2021**, *1241*, 130626. https://doi.org/10.1016/j.molstruc.2021.130626.

Scheme

Scheme 1 is available in supplementary section.

Figures

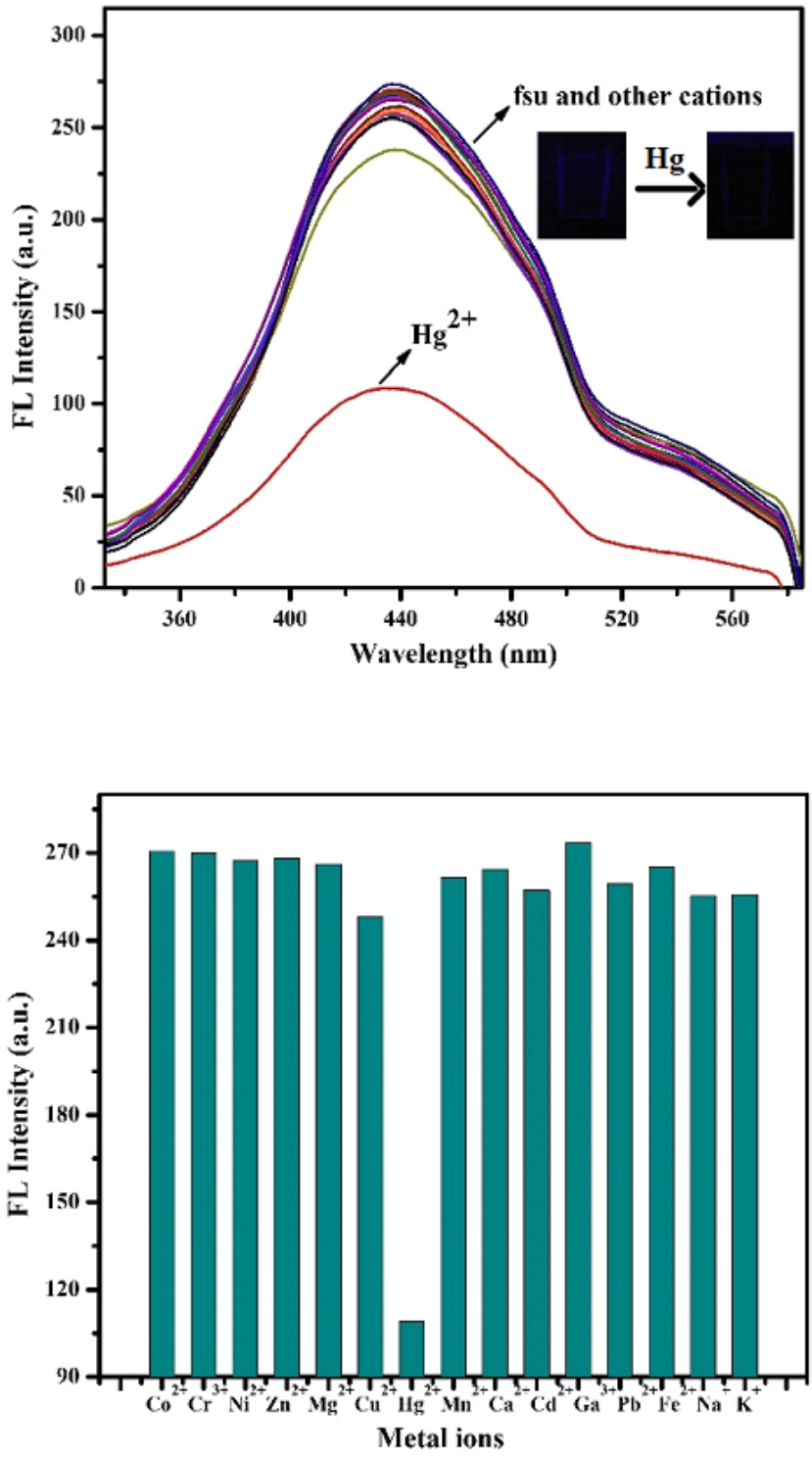

Figure 1

(a) Fluorescence intensity pattern of chemosensor FSU (8 10^{-5} M) in the presence of various cations (8 10^{-4} M) in DMSO/water (95/5, v/v) solution, **(b)** Fluorescence intensity pattern of chemosensor FSU with the existence of all other metal cations in DMSO/water (95/5, v/v) system (λ_{em}=440 nm, λ_{ex}=305 nm)

Figure 2

(a) Metal ion competitive study of the FSU-Hg^{2+} chemosensor over other different metal ions in DMSO/water (95/5, v/v) medium **(b)** the fluorescence spectra of FSU with the increasing concentration of Hg^{2+} in DMSO/water (95/5, v/v) system (λ_{em}=440 nm, λ_{ex}=305 nm)

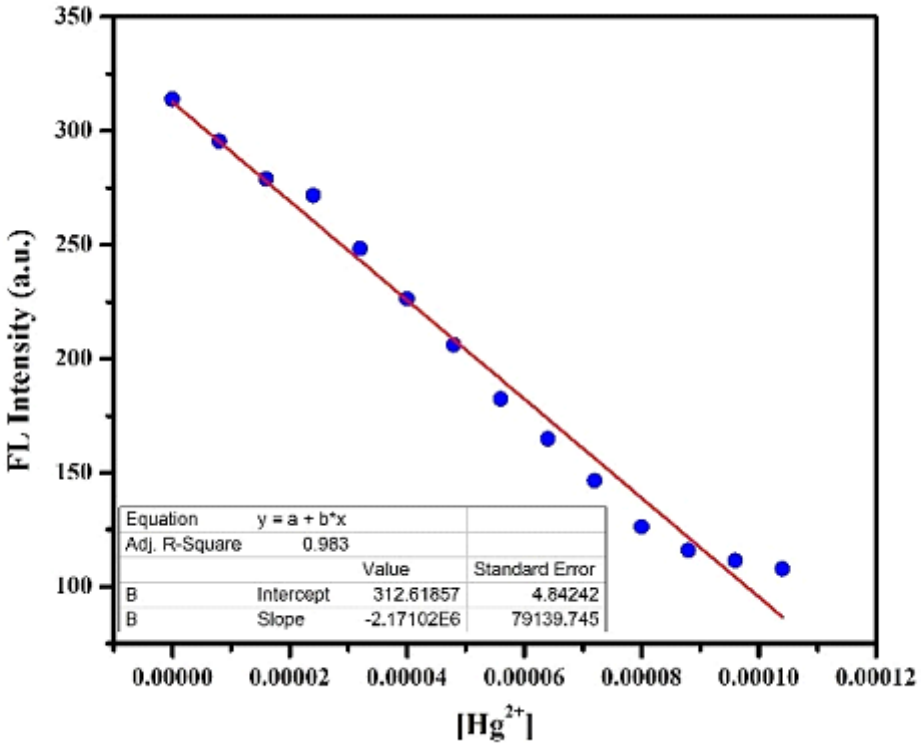

Figure 3

Diagram showing the emission intensities of chemosensor FSU against various Hg^{2+} ion concentrations (λ_{em}=440 nm, λ_{ex}=305 nm).

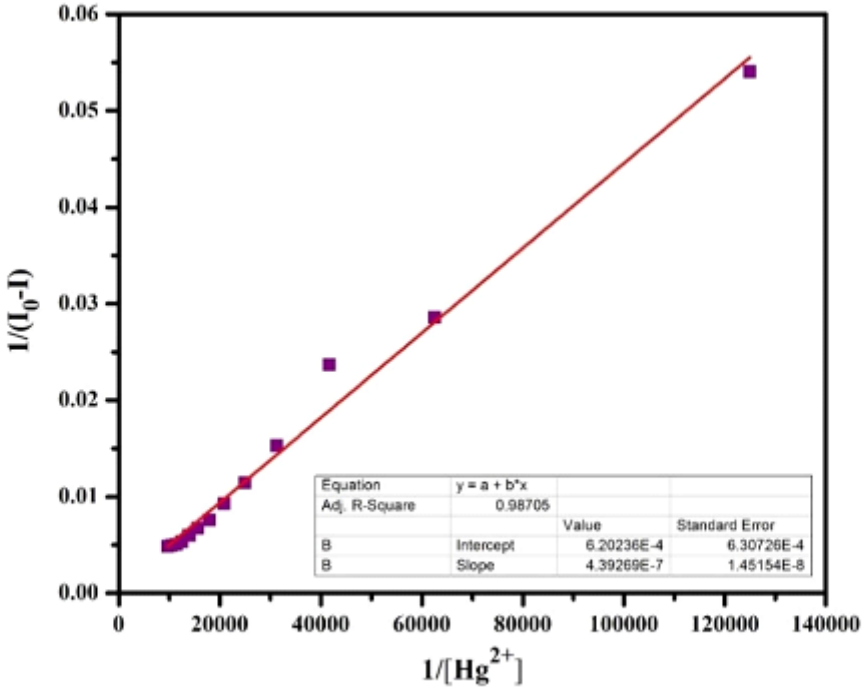

Figure 4

B-H plot of $1/(I_0-I)$ versus $1/[Hg^{2+}]$ on the basis of 2:1 stoichiometry between chemosensor FSU-Hg^{2+} complex (λ_{em}=440 nm, λ_{ex}=305 nm)

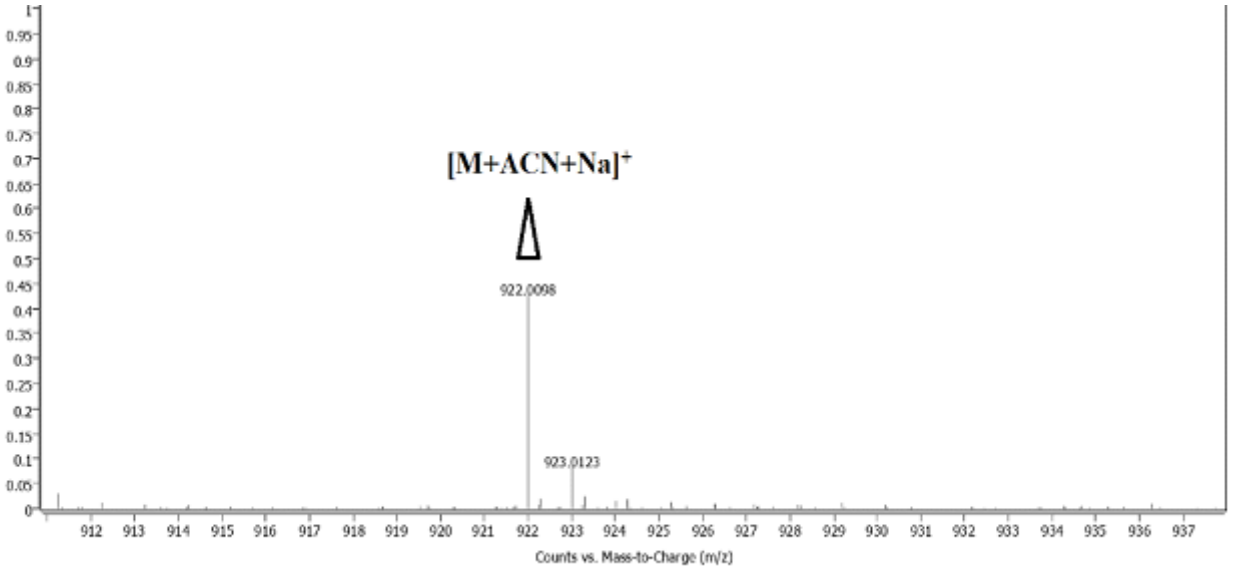

Figure 5

HR-MS spectrum of chemosensor FSU-Hg^{2+} complex

Figure 6

Job's plot of chemosensor FSU-Hg^{2+} complex in DMSO/water (95/5, v/v) medium.

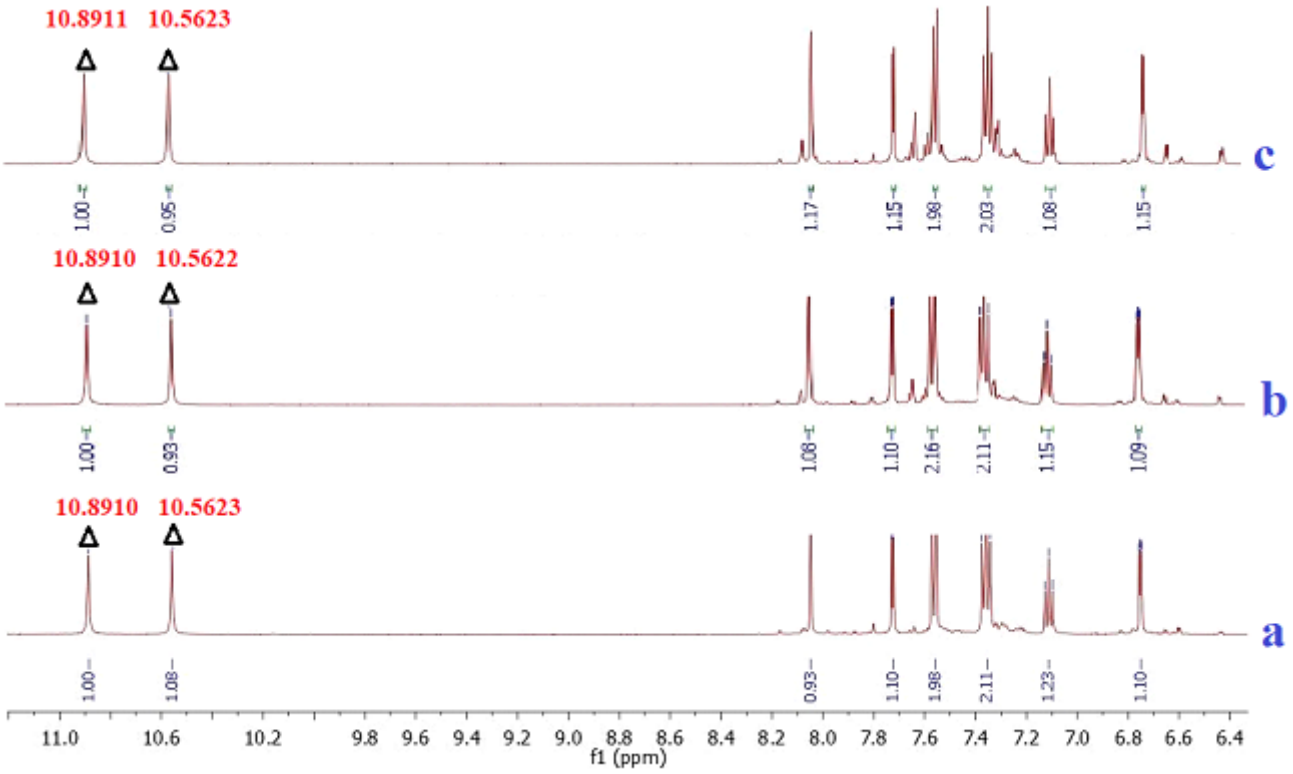

Figure 7

^{1}H NMR titration spectra of FSU with the addition of (a) 0.0 (b) 1.5 (c) 3.0 equiv. of Hg^{2+} in DMSO-d6.

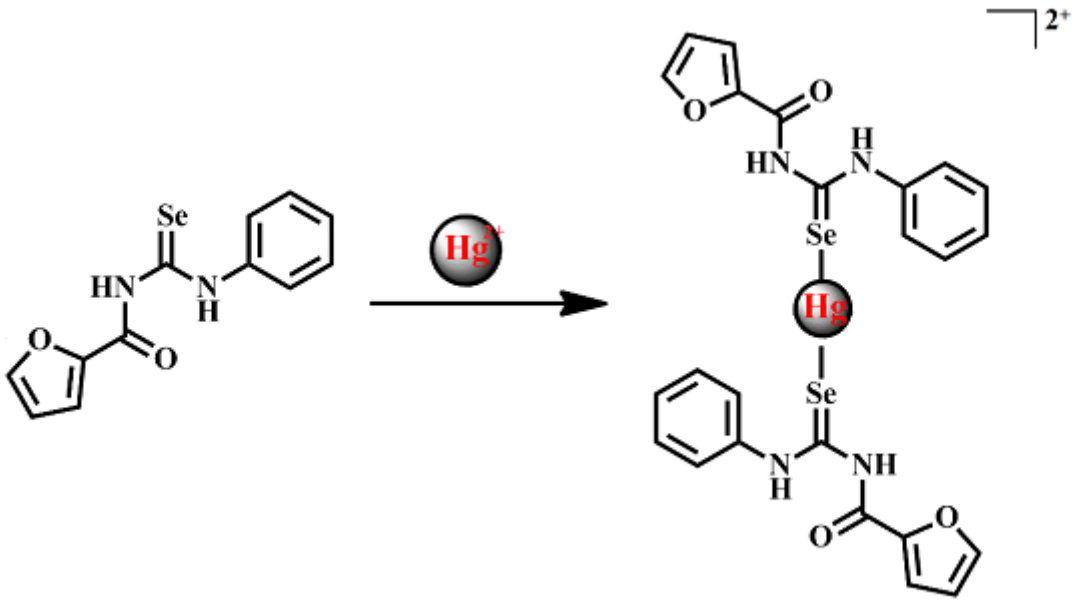

Figure 8

The proposed binding mechanism of chemosensor FSU and mercury (II) complex in DMSO/water solution (95/5, v/v)

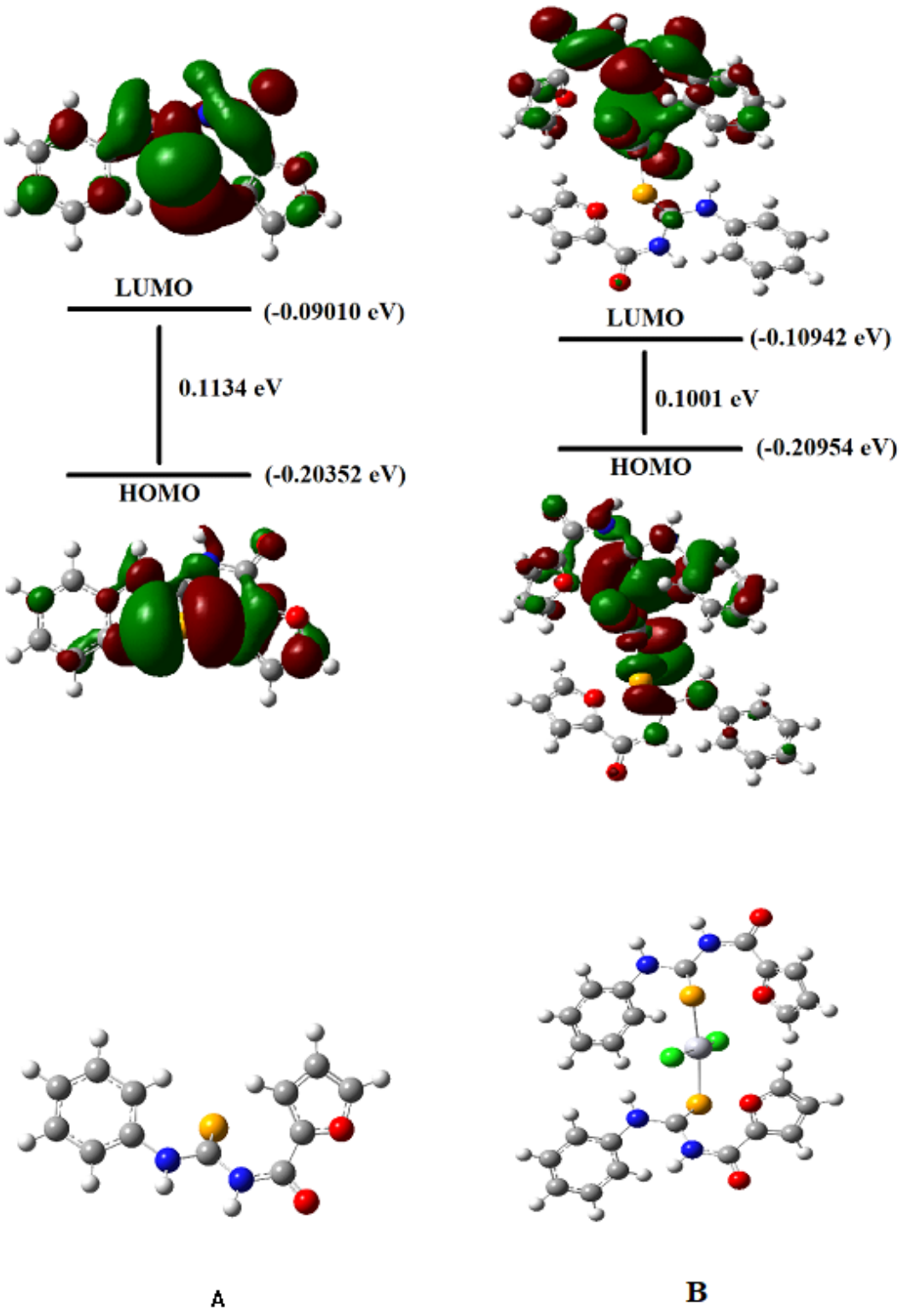

Figure 9

HOMO and LUMO energy levels of FSU (**A**) and FSU-Hg^{2+} complex (**B**)

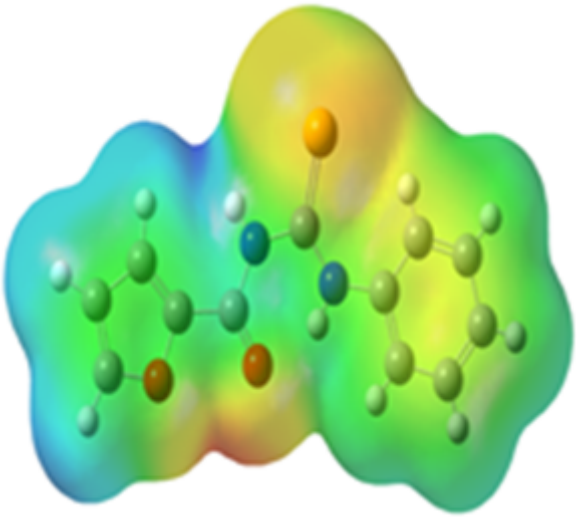

Figure 10

The MEP of FSU calculated using B3LYP/6-31G (d, p) basis set.

Supplementary Files

This is a list of supplementary files associated with this preprint. Click to download.

- Supplementarydata.docx
- floatimage1.png
- Scheme01.png